第41卷第1期 计 算 力 学 学 报 Vol. 41, No. 1
2024 年 2 月 Chinese Journal of Computational Mechanics February 2024

DOI: 10.7511/jslx20231110002

Analyzing wrinkling instabilities in constrained dielectric elastomers: A symplectic eigenvalue approach

ZHANG Teng*

(Department of Mechanical and Aerospace Engineering, Syracuse University, NY 13244, USA)

Abstract: Symplectic elasticity has been widely used to find the exact solutions of various boundary value problems in elasticity, compute the surface wave modes, and predict surface wrinkles in multilayer hyper-elastic films. Here, we show that the symplectic analysis framework can also be applied to surface wrinkles in constrained dielectric elastomers, where the mechanical deformation is tightly coupled with the electric field. The critical voltage for wrinkles can be solved as a symplectic eigenvalue problem after introducing the dual variables to the primary variables of mechanical and electric displacement vectors. We employ the extended Wittrick-Williams (W-W) algorithm and precise integration method to solve the eigenvalues of the formulated symplectic eigenvalue problem accurately and efficiently. The symplectic analysis is validated by comparing the wrinkle voltage and wavenumber with benchmark results of wrinkles with and without surface energy. The symplectic framework is concise and applicable to other instability problems such as layered dielectric elastomers, magnetoelastic instabilities and the micro- and macro-instabilities of laminated composite structures.

Key words: symplectic; dielectric elastomers; wrinkling; eigenvalue analysis

1 Introduction

Symplectic elasticity, pioneered by Prof. Zhong et al.[1-4], represents a theorical framework of transferring elliptic partial differential equations into Hamiltonian systems of first ordinary differential equations via mimicking the time coordinate with one spatial coordinate. Over the past three decades, symplectic analysis has significantly advanced the analysis of various complex problems, from solving boundary value problems in elasticity[4-7] and plates[8-11] to understanding the wave propagation in layered materials[12-15] and predicting surface wrinkles in multilayer hyper-elastic films[16,17]. Recent efforts have been devoted to extending the analysis beyond purely mechanical systems by incorporating multphysics couplings, such as guided waves in magneto-electro-elastic laminated structures[18].

The analysis becomes even more challenging when themultiphysics interactions are coupled with large deformation. Examples include surface wrinkles and creases in a constrained dielectric elastomer layer[19-23], where the voltage difference between the top and bottom surface and the mechanical confinement create driving force for the surface instabilities. The instability induced surface patterns can dynamically change the surface topography and generate new functions, such as on-demand fluorescent patterning[24]. The surface instabilities, including the critical wrinkling voltage and wrinkling wavelength have also been shown modulated by surface energy[23,25,26], an important factor for very soft materials. The rich deformation patterns and promising applications have attracted numerous theoretical attentions to investigate the surface instabilities in the dielectric elastomers[25-29].

Here, we will show that the analysis of surface wrinkling in constrained dielectricelastoemers can be

Received by: 2023-11-10; **Revised by**: 2023-11-24.

Corresponding authors: ZHANG Teng* (1985-), Male, Associate Professor
(E-mail: tzhang48@syr.edu).

formulated as a symplectic eigenvalue problem, which can be accurately and efficiently solved by leveraging the powerful tool developed in the literature. The rest of the paper is organized as follows. Section 2 is for the development of symplectic eigenvalue equations for wrinkling instabilities of a dielectric elastomer layer. We briefly reviewed the extended W-W algorithm for solving symplectic eigenvalue problems in Section 3. In Section 4, we apply the symplectic method to analyze the critical wrinkling voltage of a constrained dielectric elastomers with and without surface tension. Some concluding remarks are drawn in Section 5.

2 Symplectic equations for wrinkling instabilities in a dielectric elastomer layer

We consider one-dimensional (1D) wrinkling instabilities in a two-dimensional (2D) dielectric elastomer layer (Fig.1), where surface wrinkles can be triggered by applying a voltage to the structure. The wrinkling instabilities have been widely studied through experiments, theories, and simulations. Here we derive asymplectic eigenvalue analysis framework for the problem and provide a powerful and accurate numerical method to solve the highly nonlinear transcendent equations associated with the eigenvalue problems. We adopt the same free energy functions for ideal dielectric elastomer in previous studies[29,30] and assume the dielectric elastomer layer under plane strain condition, such that

$$W=\frac{\mu}{2}(I_1-3-2\ln J)+\frac{1}{2}\lambda_L(J-1)^2-\frac{\epsilon}{2}JF^{-1}_{Ki}F^{-1}_{Li}E_KE_L \tag{1}$$

where μ is the shear modulus, λ_L the Lame constant, ϵ the permeability, $I_1=\lambda_1^2+\lambda_2^2+1$, λ_i the principal stretches and J the determinant of the deformation gradient tensor $\boldsymbol{F}=\partial\boldsymbol{x}/\partial\boldsymbol{X}$, $\boldsymbol{X}$ and $\boldsymbol{x}$ denote the reference and deformed configurations, respectively, $\boldsymbol{E}=-(\partial\phi/\partial\boldsymbol{X})$ the electric field vector at the reference configuration, and ϕ the electric potential.

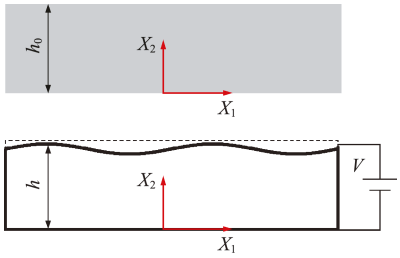

Fig. 1 Problem setup of the wrinkles in constrained dielectric elastomer (Top is the reference state of the dielectric elastomer layer and bottom is the schematic of the wrinkled dielectric elastomer layer at the critical voltage)

An augmented free energy function can be derived from Eq.(1) by employing the electric displacement, $\boldsymbol{D}=\partial W/\partial\boldsymbol{E}$ as an independent variable through the Legendre-type transform[31]

$$\Omega=\frac{\mu}{2}(I_1-3-2\ln J)+\frac{1}{2}\lambda_L(J-1)^2+\frac{1}{2\epsilon}J^{-1}\boldsymbol{D}\cdot(\boldsymbol{CD}) \tag{2}$$

where $\boldsymbol{C}=\boldsymbol{F}^{\mathrm{T}}\boldsymbol{F}$ is the right Cauchy-Green tensor.

In this work, we will develop thesymplectic analysis based on free energy function in Eq.(2). It has been shown by Zhang et al.[18] that the positive definite nature of the free energy function is critical for the eigenvalue solver used here. It should be noticed that symplectic eigenvalue problems can still be formed using Eq.(1).

The first Piola-Kirchhoff stress and electric filed vector can be expressed as

$$\boldsymbol{P}=\mu\boldsymbol{F}-[\mu-\lambda_L J(J-1)]\boldsymbol{F}^{-\mathrm{T}}+\epsilon^{-1}J^{-1}\boldsymbol{F}(\boldsymbol{D}\otimes\boldsymbol{D})-\frac{1}{2}\epsilon^{-1}J^{-1}(\boldsymbol{D}\cdot(\boldsymbol{CD}))\boldsymbol{F}^{-\mathrm{T}} \tag{3}$$

$$\boldsymbol{H}=\frac{1}{\epsilon}J^{-1}\boldsymbol{CD} \tag{4}$$

where $\boldsymbol{D}\otimes\boldsymbol{D}$ represents the tensor product of vector $\boldsymbol{D}$ and $\boldsymbol{D}\cdot(\boldsymbol{CD})$ denotes dot product of the vector $\boldsymbol{D}$ and $\boldsymbol{CD}$.

The governing equations of the system are,

$$\mathrm{Div}\boldsymbol{P}=\boldsymbol{0},\ \mathrm{Div}\boldsymbol{D}=\boldsymbol{0},\ \mathrm{Curl}\boldsymbol{E}=\boldsymbol{0} \tag{5}$$

To analyze the wrinkling solution, we decouple the deformation mapping and electric potential into a uniform solution and a perturbed solution[29], suchthat

$$x_i=\delta_{ij}X_j+(\lambda_2-1)\delta_{i2}X_2+\alpha u_i(X_1,X_2) \tag{6}$$

$$\phi=\frac{V}{h_0}(X_2)+\alpha\varphi(X_1,X_2) \tag{7}$$

where u_i denotes the perturbed displacements, φ

represents perturbed electric potential field, and α is a dimensionless variable. The uniform deformation can be large while the perturbed solution is small, corresponding to a small α.

Since electric displacement is the independent variables, we further decouple it into a summation of a uniform and perturbed solution,

$$\boldsymbol{D}=\begin{bmatrix}D_1^0\\D_2^0\end{bmatrix}+\alpha\begin{bmatrix}\xi_1\\\xi_2\end{bmatrix} \tag{8}$$

We compute the Taylor series of the electric field vector and the first Piola-Kirchhoff stress in terms of α and keep the 0^{th} and 1^{st} order, which are given by

$$\boldsymbol{E}=\boldsymbol{E}^0+\alpha\boldsymbol{E}^1,\ \boldsymbol{P}=\boldsymbol{P}^0+\alpha\boldsymbol{P}^1 \tag{9,10}$$

where $\boldsymbol{E}^0,\boldsymbol{E}^1,\boldsymbol{P}^0,\boldsymbol{P}^1$ are given in Appendix A.

Before wrinkle instabilities occur, the stress-free boundary condition of the top surface, such as $P_{22}^0=0$, leads to the following equation

$$\mu\lambda_2-\Pi_0\lambda_2^{-1}+\frac{1}{2}\epsilon^{-1}(D_2^0)^2=0 \tag{11}$$

where $\Pi_0=\mu-\lambda_L\lambda_2(\lambda_2-1)$. The solution of Eq.(11) gives the stretching ratio (λ_2) along the x_2 for a given electric displacement D_2^0

$$\lambda_2=\left\{\left[\left(\lambda_L-\frac{1}{2}\epsilon^{-1}(D_2^0)^2\right)^2+4(\lambda_L+\mu)\mu\right]^{1/2}+\left(\lambda_L-\frac{1}{2}\epsilon^{-1}(D_2^0)^2\right)\right\}\Big/\left[2(\lambda_L+\mu)\right] \tag{12}$$

Noting that the electric field can also be computed from the electric potential as $\boldsymbol{E}=-\mathrm{Grad}(\phi)$, we can find the relation between D_2^0 and the electric potential as

$$D_2^0=-\epsilon\lambda_2^{-1}h_0^{-1}V \tag{13}$$

In our analysis, we will use D_2^0 as an independent variable and the corresponding electric potential will be computed using Eq.(13) after λ_2 is solved in Eq.(12).

We next analyze the equilibrium equations of the 1^{st} order of α. Since we focus on the 2D wrinkles, $\mathrm{Curl}\boldsymbol{E}=\boldsymbol{0}$ only has one non-zero component, leading to the following equations

$$L_{111}u_{1,11}+L_{122}u_{1,22}+L_{212}u_{2,12}+\epsilon^{-1}(D_2^0)(\lambda_2^{-1}\xi_{1,2}-\lambda_2\xi_{2,1})=0 \tag{14}$$

$$L_{222}u_{2,22}+L_{211}u_{2,11}+L_{112}u_{1,12}=0 \tag{15}$$

$$\epsilon^{-1}(\xi_{2,1}\lambda_2-\xi_{1,2}\lambda_2^{-1}-D_2^0\lambda_2u_{1,11}-D_2^0\lambda_2^{-1}u_{1,22})=0 \tag{16}$$

$$\partial\xi_1/\partial X_1+\partial\xi_2/\partial X_2=0 \tag{17}$$

where $L_{111}=(\lambda_L\lambda_2^2+2\mu+\epsilon^{-1}(D_2^0)^2\lambda_2)$

$L_{122}=(\mu+\epsilon^{-1}\lambda_2^{-1}(D_2^0)^2)$

$L_{211}=\mu, L_{222}=(\lambda_L+\mu+\mu\lambda_2^{-2})$

$L_{112}=L_{212}=(\lambda_L\lambda_2+\mu\lambda_2^{-1})$

Eqs.(14,15) are the stress equilibrium equation and Eqs.(16,17) are the Maxwell's equations, corresponding to $\mathrm{Curl}\boldsymbol{E}=\boldsymbol{0}$ and $\mathrm{Div}\boldsymbol{D}=\boldsymbol{0}$, respectively. The boundary conditions are given by

$$u_1(X_1,0)=u_2(X_1,0)=\varphi(X_1,0)=0 \tag{18}$$

$$P_{12}(X_1,h_0)=\varphi(X_1,h_0)=0$$

$$P_{22}(X_2,h_0)=\gamma u_{1,22} \tag{19}$$

where γ is the surface energy and φ is a function of u_1, u_2, and ξ_1, ξ_2. Similar equations have been derived before for fully incompressible dielectric elastomers[32,33].

To search for the wrinkling solution, we express the variables in Fourier space, such that

$$u_1=\exp(ikX_1)U_1(X_2),\ u_2=\exp(ikX_1)U_2(X_2)$$

$$\xi_1=\exp(ikX_1)\Xi_1(X_2),\ \xi_2=\exp(ikX_1)\Xi_2(X_2)$$

$$\varphi=\exp(ikX_1)\Psi(X_2)$$

where k is the wavenumber. It should be noted that the Fourier modes only apply to the onset instability of the surface. It can be seen from Eq.(19) that Ξ_1 is not an independent variable and can be expressed as

$$\Xi_1=i(k^{-1})\Xi_2' \tag{20}$$

In Fourier space, $\Psi(X_2)$ can be solved from Eq.(9) as

$$\Psi=-\epsilon^{-1}k^{-2}\lambda_2^{-1}\Xi_2'+(\epsilon^{-1}D_2^0\lambda_2^{-1}k^{-1})iU_1'-\epsilon^{-1}D_2^0U_2 \tag{21}$$

We further multiply (ik^{-1}) to Eq.(16) and rearrange equilibrium equations in Eqs.(14～16) in the Fourier space as

$$\boldsymbol{K}_{22}\boldsymbol{q}''+(\boldsymbol{K}_{21}-\boldsymbol{K}_{12})\boldsymbol{q}'-\boldsymbol{K}_{11}\boldsymbol{q}=0 \tag{22}$$

where $\boldsymbol{q}=[U_1\ U_2\ \Xi_2]^{\mathrm{T}}$, $(\#)'=\mathrm{d}(\#)/\mathrm{d}X_2$, $(\#)''=\mathrm{d}^2(\#)/\mathrm{d}X_2^2$, $\boldsymbol{K}_{22}$, $\boldsymbol{K}_{21}$, $\boldsymbol{K}_{12}$, and $\boldsymbol{K}_{11}$ are given in Appendix B.

We next introduce the dual variable of $\boldsymbol{q}$

$$\boldsymbol{p}=-(\boldsymbol{K}_{22}\boldsymbol{q}'+\boldsymbol{K}_{21}\boldsymbol{q}) \tag{23}$$

The physical meanings of the dual variables are given as follows

$$p_1=-\widetilde{P}_{12},\ p_2=-\widetilde{P}_{22}+\epsilon^{-1}D_2^0\Xi_2,\ p_3=\Psi+\epsilon^{-1}D_2^0U_2 \tag{24}$$

where $\widetilde{P}_{12}$ and $\widetilde{P}_{22}$ are the Fourier transformations of

the P_{12} and P_{22}, respectively. The governing equations can then be expressed in terms of state variable $\mathbf{V}=[\boldsymbol{q},\boldsymbol{p}]$ as

$$\mathbf{V}'=\boldsymbol{H}\mathbf{V},\ \boldsymbol{H}=\begin{bmatrix}\boldsymbol{H}_{qq} & \boldsymbol{H}_{qp}\\ \boldsymbol{H}_{pq} & \boldsymbol{H}_{pp}\end{bmatrix} \tag{25}$$

where
$$\boldsymbol{H}_{qq}=-\boldsymbol{H}_{pp}^{H}=-\mathbf{K}_{22}^{-1}\mathbf{K}_{21}$$
$$\boldsymbol{H}_{pq}=-(\mathbf{K}_{11}-\mathbf{K}_{12}\mathbf{K}_{22}^{-1}\mathbf{K}_{21})$$
$$\boldsymbol{H}_{qp}=-\mathbf{K}_{22}^{-1}$$

It can be verified that H is a Hamiltonian matrix that satisfies $\boldsymbol{\Lambda}^{-1}\boldsymbol{H}\boldsymbol{\Lambda}=-\boldsymbol{H}^{H},\boldsymbol{\Lambda}=\begin{bmatrix}\mathbf{0} & \boldsymbol{I}\\ -\boldsymbol{I} & \mathbf{0}\end{bmatrix}$ with $\boldsymbol{I}$ as the identity matrix.

The boundary conditions in the Fourier space can be described as

$$U_1(0)=0,\ U_2(0)=0,\ p_3(0)=0 \tag{26}$$

$$p_1(h_0)=0,\ p_2(h_0)=\epsilon^{-1}D_2^0\Xi_2+\gamma k^2U_2$$
$$p_3(h_0)=\epsilon^{-1}D_2^0U_2 \tag{27}$$

3 Extended Wittrick-Williams (W-W) algorithm for symplectic eigenvalue analysis

The symplectic eigenvalue problems defined in Eqs.(25～27) can be effectively and accurately solved by integrating the precise integration method (PIM) and the extended Wittrick-Williams (W-W) algorithm[34]. The algorithm has been successfully applied to various engineering applications, such as waves propagation in multilayered structures[12-15], surface wrinkles in neo-Hookean bilayer structures[16,17], and guided waves in magneto-electro-elastic laminated structures[18]. Here, we will briefly review the PIM method and W-W algorithm and refer readers to literatures[15,18] for more detailed analysis.

W-W algorithm is based on the eigenvalue count, which represents the number of eigenvaluesin the system under given boundary conditions. The algorithm first rewrites Eq.(25) in the mixed energy format. For a layer within the interval $[t_1,t_{\mathrm{II}}]$, if state variables $\boldsymbol{q}_1,\boldsymbol{p}_{\mathrm{II}}$ are given, the rest state variables $\boldsymbol{q}_{\mathrm{II}},\boldsymbol{p}_1$ can be expressed as

$$\boldsymbol{q}_{\mathrm{II}}=\mathbf{F}_1\boldsymbol{q}_1-\mathbf{G}_1\boldsymbol{p}_{\mathrm{II}},\ \boldsymbol{p}_1=\boldsymbol{Q}_1\boldsymbol{q}_1+\mathbf{F}_1^{H}\boldsymbol{p}_{\mathrm{II}} \tag{28}$$

where $\mathbf{F}_1,\mathbf{G}_1$ and $\boldsymbol{Q}_1$ are complex matrices and can be computed from the following differential equations

$$\mathbf{F}_1'=(\boldsymbol{H}_{qq}+\mathbf{G}_1\boldsymbol{H}_{pq})\mathbf{F}_1 \tag{29a}$$

$$\mathbf{G}_1'=\boldsymbol{H}_{qq}\mathbf{G}_1+\mathbf{G}_1\boldsymbol{H}_{qq}^{H}+\mathbf{G}_1\boldsymbol{H}_{pq}\mathbf{G}_1-\boldsymbol{H}_{qp} \tag{29b}$$

$$\boldsymbol{Q}_1'=-\mathbf{F}_1^{H}\boldsymbol{H}_{pq}\mathbf{F}_1 \tag{29c}$$

where $\boldsymbol{H}_{qq},\boldsymbol{H}_{pq}$ and $\boldsymbol{H}_{qp}$ are given in Eq.(25) and the initial conditions are $\mathbf{F}_1(t_1)=\mathbf{I},\mathbf{G}_1(t_1)=\boldsymbol{Q}_1(t_1)=\mathbf{0}$. We define the eigenvalue count $J_1(D_2^0;k)$ as the eigenvalue count with the specified boundary conditions of $\boldsymbol{q}_1=\mathbf{0}$ and $\boldsymbol{q}_{\mathrm{II}}=\mathbf{0}$ for a given wavenumber k.

For two consecutive intervals $[t_1,t_{\mathrm{II}}]$ and $[t_{\mathrm{II}},t_{\mathrm{III}}]$ with given $J_1,\mathbf{F}_1,\mathbf{G}_1$ and $\boldsymbol{Q}_1$ for layer I as well as $J_{\mathrm{II}},\mathbf{F}_{\mathrm{II}},\mathbf{G}_{\mathrm{II}}$ and $\boldsymbol{Q}_{\mathrm{II}}$ for layer II, the relation for $\boldsymbol{q}_1,\boldsymbol{p}_{\mathrm{III}}$ and $\boldsymbol{q}_{\mathrm{III}},\boldsymbol{p}_1$ can be described as[12,13,15,18]

$$\mathbf{F}_{\mathrm{III}}=\mathbf{F}_{\mathrm{II}}(\boldsymbol{I}+\mathbf{G}_1\boldsymbol{Q}_{\mathrm{II}})^{-1}\mathbf{F}_{\mathrm{II}} \tag{30a}$$

$$\mathbf{G}_{\mathrm{III}}=\mathbf{G}_{\mathrm{II}}+\mathbf{F}_{\mathrm{II}}(\mathbf{G}_1^{-1}+\boldsymbol{Q}_{\mathrm{II}})^{-1}\mathbf{F}_{\mathrm{II}}^{H} \tag{30b}$$

$$\boldsymbol{Q}_{III}=\boldsymbol{Q}_{II}+\mathbf{F}_{\mathrm{II}}^{H}(\mathbf{G}_1+\boldsymbol{Q}_{\mathrm{II}}^{-1})^{-1}\mathbf{F}_1 \tag{30c}$$

and the eigenvalue count

$$J_{\mathrm{III}}(D_2^0;k)=J_1(D_2^0;k)+J_{\mathrm{II}}(D_2^0;k)+s\{(\mathbf{G}_1^{-1}+\boldsymbol{Q}_{\mathrm{II}}+\mathbf{F}_{\mathrm{II}}^{H}\mathbf{G}_{\mathrm{II}}^{-1}\mathbf{F}_{\mathrm{II}})\} \tag{31}$$

where $s\{\#\}$ denotes the number of negative eigenvalues in matrix $\#$.

In general, the eigenvalue count for a finite layer is unknown. To address this issue, the given layer structure will first be divided into it into 2^N very small sub-layer and then combined through the precise integration method (PIM). A large N is chosen to make the finest sub-layer thin enough to have a 0 eigenvalue count ($J_{0,h}^{N}=0$). The matrix $\mathbf{F}_{0,h}^{N},\mathbf{G}_{0,h}^{N}$ and $\boldsymbol{Q}_{0,h}^{N}$ in the finest layer can be calculated with truncated Taylor series (see Appendix C). With this information and the combination process of two intervals to into a larger one (see Appendix C), it only takes N^{th} iterations to calculate the eigenvalue count of a finite uniform layer, which forms an efficient and accurate method and known as the precise integration method (2^N algorithm)[13].

After applying the PIM method, we can obtain the relationships of the state variable of the dielectric elastomer layer between the top and bottom surfaces as

$$\boldsymbol{p}_0=-\boldsymbol{Q}_{0,h}\boldsymbol{q}_0+\mathbf{F}_{0,h}^{H}\boldsymbol{p}_h \tag{32a}$$

$$\boldsymbol{q}_h=\mathbf{F}_{0,h}\boldsymbol{q}_0+\mathbf{G}_{0,h}\boldsymbol{p}_h \tag{32b}$$

We first compute the eigenvalue count due to the boundary condition at $X_2=h$, which can be written in the matrix form as

$$\boldsymbol{p}_h=\mathbf{R}_s\boldsymbol{q}_h,\ \mathbf{R}_s=\begin{bmatrix}0 & 0 & 0\\ 0 & \gamma k^2 & \epsilon^{-1}\mathrm{D}_2^0\\ 0 & \epsilon^{-1}\mathrm{D}_2^0 & 0\end{bmatrix} \tag{33}$$

From Eq.(37b), we can further obtain by noticing $\boldsymbol{q}_0=\mathbf{0}$

$$\boldsymbol{p}_h=\mathbf{G}_{0,h}^{-1}\boldsymbol{q}_h \tag{34}$$

The total stiffness matrix at the top surface can be expressed as

$$\boldsymbol{p}_h=\mathbf{R}_h\boldsymbol{q}_h,\ \text{with}\ \mathbf{R}_h=\mathbf{G}_{0,h}^{-1}-\mathbf{R}_s \tag{35}$$

Therefore, the eigenvaluecount by incorporating the top surface boundary condition is

$$\mathrm{J}_1=\mathrm{J}_0+\mathrm{sign}(\mathbf{G}_{0,h}^{-1}-\mathbf{R}_s) \tag{36}$$

We next consider the boundary condition at $X_2=0$ and solve stiffness matrix from Eqs.(32a, 32b, 33) as

$$\boldsymbol{p}_0=-\mathbf{R}_0\boldsymbol{q}_0 \tag{37}$$

where $\mathbf{R}_0=(\boldsymbol{Q}_{0,h}-\boldsymbol{F}_{0,h}^H(\boldsymbol{I}-\mathbf{R}_s\boldsymbol{G}_{0,h})^{-1}\mathbf{R}_s\boldsymbol{F}_{0,h})$.

At $X_2=0$, the new boundary condition is $p_3=0$, leading the final eigenvalue count as

$$\mathrm{J}_2=\mathrm{J}_1+\mathrm{sign}((R_0)_{33}) \tag{38}$$

4　Wrinkling analysis in the constrained dielectric elastomer layer

In this section, we apply the developedsymplectic eigenvalue analysis to the computation of surface wrinkling in the constrained dielectric elastomer layer. It has been shown that the bulk modulus play an important role in determining the critical voltage. We first compute the critical voltage as a function of the wave number for two representative materials with different Lame constants and same shear modulus and set the surface energy $\gamma=0$. As shown in Fig.2, the normalized critical voltage is larger for the case with a larger bulk modulus. The large bulk modulus can be seen as a good approximation of incompressible condition. Our simulation shows that the critical voltage reaches a plateau of $\sqrt{2}$ at the short-wave limit, in great agreement with previous analytical solutions[27].

As shown in Fig.2, the critical voltage monotonically decreases with the wrinkle wavelength and eventually reaches a plateau. We next focus on the short-wave limit case, which is realized in the numerical simulations by setting a large wavenumber of $100h_0^{-1}$. We vary the bulk modulus and show the normalized critical voltage continuously increases as the increase of the bulk modulus and has as limit of $\sqrt{2}$ (Fig.3). The comparison between the symplectic analysis and analytical solutions[27,29] is also presented in Fig.3, showing very good agreement between each other. It should be noticed that the analytical solution is based on approximated theory, which is the reason of the small difference shown in Fig.3.

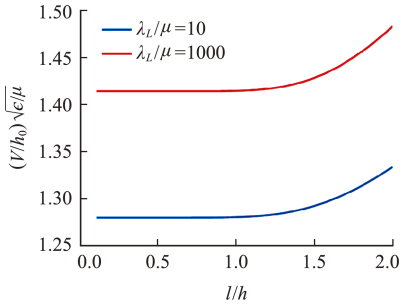

Fig. 2　Bifurcation eigenvalue spectrum for the two neo-Hookean layer problems with different Lame constants

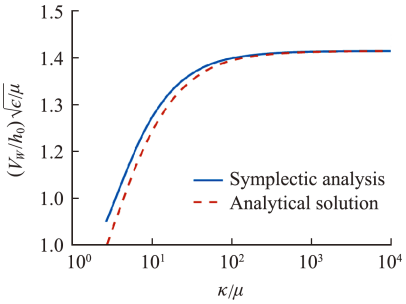

Fig. 3　Critical voltage V_W for the onset of wrinkling (orange dashed line is the analytic solution by Huang[27])

Lastly, we examine the effect of surface energy on the critical voltage for surface wrinkling. Our method is very easy and natural to incorporate the surface energy term, which is given by the γk^2 term in $\mathbf{R}_S$ in Eq.(38). A few representative cases are shown in Fig.4. For a finite surface energy, the critical voltage first decreases as the decreases with the wavelength and then increases. This is due to the small wavelength tends to increase the surface area and thus the system energy. Therefore, a minimum voltage will exist. Our results are also in great agreement with the previous analysis[26].

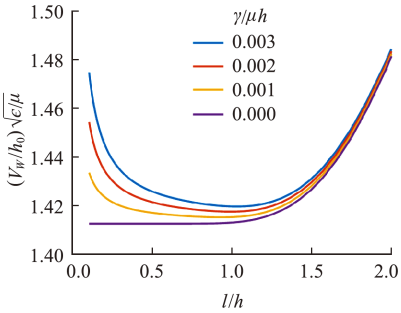

Fig. 4　Effect of surface energy on the onset wrinkling bifurcation

5 Concluding remarks

We have successfully demonstrated the applicability of thesymplectic analysis framework in investigating surface wrinkles in constrained dielectric elastomers, where the mechanical deformation is tightly coupled with the electric field. The unique symplectic structure makes it possible to solve the nontrivial boundary value problem efficiently and accurately in the eigenvalue analysis of wrinkles through the extended W-W algorithm and the precise integration method. We validate that the symplectic analysis can obtain the exact wrinkle voltage and wavenumber compared with benchmark results of wrinkles with and without surface energy. The single layer analysis in the current work can be easily extended to multilayer structures with and without periodical boundary condition, which is ready for the analysis of the stability of layered electroactive polymers[35-37] and micro- and macro-instabilities in composite laminated structure instabilities[38-43]. Furthermore, the concise mathematical structure of the symplectic analysis allows it adaptable to various multiphysics coupling problems, such as the exploration of magnetoelastic instabilities[44-46].

Acknowledgments

The author expresses sincere gratitude to Prof. Wanxie Zhong for invaluable advising and support, which provided the foundation for this research. Additionally, the author acknowledges the guidance and assistance provided by Prof. Qiang Gao.

Appendix A Taylor series of the electric field vector and the firstPiola-Kirchhoff stress

$$\boldsymbol{E}^0=\epsilon^{-1}\begin{bmatrix}0\\ D_2^0\lambda_2\end{bmatrix} \tag{A1}$$

$$\boldsymbol{E}^1=\epsilon^{-1}\begin{bmatrix}\xi_1\lambda_2^{-1}+D_2^0\lambda_2^{-1}(u_{1,2}+\lambda_2 u_{2,1})\\ \xi_2\lambda_2+D_2^0(u_{2,2}-\lambda_2 u_{1,1})\end{bmatrix} \tag{A2}$$

$$P_{11}^0=\lambda_L\lambda_2(\lambda_2-1)-\frac{1}{2}\epsilon^{-1}\lambda_2(D_2^0)^2 \tag{A3a}$$

$$P_{22}^0=\mu\lambda_2-\Pi_0\lambda_2^{-1}+\frac{1}{2}\epsilon^{-1}(D_2^0)^2 \tag{A3b}$$

$$P_{12}^0=P_{21}^0=0 \tag{A3c}$$

$$P_{11}^1=(\lambda_L\lambda_2^2+2\mu+\epsilon^{-1}(D_2^0)^2\lambda_2)u_{1,1}+(2\lambda_L\lambda_2-\lambda_L-\frac{1}{2}\epsilon^{-1}(D_2^0)^2)u_{2,2}-\epsilon^{-1}(D_2^0)\lambda_2\xi_2 \tag{A4a}$$

$$P_{12}^1=(\mu+\epsilon^{-1}\lambda_2^{-1}(D_2^0)^2)u_{1,2}+\Big(\frac{1}{2}\epsilon^{-1}(D_2^0)^2+\Pi_0\lambda_2^{-1}\Big)u_{2,1}+\epsilon^{-1}(D_2^0)\lambda_2^{-1}\xi_1 \tag{A4b}$$

$$P_{21}^1=\mu u_{2,1}+\Big(\frac{1}{2}\epsilon^{-1}(D_2^0)^2+\Pi_0\lambda_2^{-1}\Big)u_{1,2}+\epsilon^{-1}D_2^0\xi_1 \tag{A4c}$$

$$P_{22}^1=(\lambda_L+\mu+\mu\lambda_2^{-2})u_{2,2}+\Big(\lambda_L(2\lambda_2-1)-\frac{1}{2}\epsilon^{-1}(D_2^0)^2\Big)u_{1,1}+\epsilon^{-1}D_2^0\xi_2 \tag{A4d}$$

Here we introduce $\Pi_0=\mu-\lambda_L\lambda_2(\lambda_2-1)$ to simplify the formula.

Appendix B The stiffness matrices in Fourier space

$$\boldsymbol{K}_{22}=\begin{bmatrix}\mu+\epsilon^{-1}\lambda_2^{-1}(D_2^0)^2 & 0 & (\epsilon^{-1}D_2^0\lambda_2^{-1}k^{-1})i\\ 0 & \lambda_L+\mu+\mu\lambda_2^{-2} & 0\\ -(\epsilon^{-1}D_2^0\lambda_2^{-1}k^{-1})i & 0 & \epsilon^{-1}k^{-2}\lambda_2^{-1}\end{bmatrix} \tag{B1}$$

$$\boldsymbol{K}_{21}=\boldsymbol{K}_{12}^H=ik\times\begin{bmatrix}0 & \frac{\epsilon^{-1}(D_2^0)^2}{2}+\Pi_0\lambda_2^{-1} & 0\\ \lambda_L(2\lambda_2-1)-\frac{\epsilon^{-1}(D_2^0)^2}{2} & 0 & 0\\ 0 & 0 & 0\end{bmatrix} \tag{B2}$$

$$\boldsymbol{K}_{11}=k^2\begin{bmatrix}\lambda_2^2\lambda_L+2\mu+\epsilon^{-1}(D_2^0)^2\lambda_2 & 0 & (\epsilon^{-1}D_2^0\lambda_2 k^{-1})i\\ 0 & \mu & 0\\ -(\epsilon^{-1}D_2^0\lambda_2 k^{-1})i & 0 & \epsilon^{-1}\lambda_2 k^{-2}\end{bmatrix} \tag{B3}$$

Appendix C The precise integration method for the eigenvalue count

At the finest level, the length of the interval is $\tau=h/2^N$. Since $\tau\ll1$, we can approximate the matrices $\boldsymbol{F}_{0,h}^N$, $\boldsymbol{G}_{0,h}^N$, and $\boldsymbol{Q}_{0,h}^N$ through Taylor series[13]

$$\boldsymbol{Q}_{0,h}^N=\boldsymbol{\theta}_1\tau+\boldsymbol{\theta}_2\tau^2+\boldsymbol{\theta}_3\tau^3+\boldsymbol{\theta}_4\tau^4 \tag{C1}$$

$$\boldsymbol{G}_{0,h}^N=\boldsymbol{\gamma}_1\tau+\boldsymbol{\gamma}_2\tau^2+\boldsymbol{\gamma}_3\tau^3+\boldsymbol{\gamma}_4\tau^4 \tag{C2}$$

$$\boldsymbol{F}_{0,h}^N=\boldsymbol{I}+\overline{\boldsymbol{F}}_j^N \tag{C3}$$

$$\overline{\boldsymbol{F}}_j^N=(\boldsymbol{\varphi}_1\tau+\boldsymbol{\varphi}_2\tau^2+\boldsymbol{\varphi}_3\tau^3+\boldsymbol{\varphi}_4\tau^4 \tag{C4}$$

where

$$\boldsymbol{\theta}_1=-\boldsymbol{H}_{pq},\ \boldsymbol{\gamma}_1=-\boldsymbol{H}_{qp},\ \boldsymbol{\varphi}_1=\boldsymbol{H}_{qq}$$

$$\boldsymbol{\theta}_2=-(\boldsymbol{\varphi}_1^H\boldsymbol{H}_{pq}+\boldsymbol{H}_{pq}\boldsymbol{\varphi}_1)/2$$

$$\boldsymbol{\gamma}_2=(\boldsymbol{H}_{qq}\boldsymbol{\gamma}_1+\boldsymbol{\gamma}_1\boldsymbol{H}_{qq}^H)/2$$

$$\boldsymbol{\varphi}_2=(\boldsymbol{H}_{qq}\boldsymbol{\varphi}_1+\boldsymbol{\gamma}_1\boldsymbol{H}_{pq})/2$$

$$\boldsymbol{\theta}_3=-(\boldsymbol{\varphi}_2^H\boldsymbol{H}_{pq}+\boldsymbol{H}_{pq}\boldsymbol{\varphi}_2+\boldsymbol{\varphi}_1^H\boldsymbol{H}_{pq}\boldsymbol{\varphi}_1)/3$$

$$\boldsymbol{\gamma}_3=(\boldsymbol{H}_{qq}\boldsymbol{\gamma}_2+\boldsymbol{\gamma}_2\boldsymbol{H}_{qq}^H+\boldsymbol{\gamma}_1\boldsymbol{H}_{pq}\boldsymbol{\gamma}_1)/3$$

$$\boldsymbol{\varphi}_3=(\boldsymbol{H}_{qq}\boldsymbol{\varphi}_2+\boldsymbol{\gamma}_2\boldsymbol{H}_{pq}+\boldsymbol{\gamma}_1\boldsymbol{H}_{pq}\boldsymbol{\varphi}_1)/3$$

$$\boldsymbol{\theta}_4=-(\boldsymbol{\varphi}_3^H\boldsymbol{H}_{pq}+\boldsymbol{H}_{pq}\boldsymbol{\varphi}_3+\boldsymbol{\varphi}_1^H\boldsymbol{H}_{pq}\boldsymbol{\varphi}_1+\boldsymbol{\varphi}_1^H\boldsymbol{H}_{pq}\boldsymbol{\varphi}_2)/3$$

$$\boldsymbol{\gamma}_4=(\mathbf{H}_{qq}\boldsymbol{\gamma}_3+\boldsymbol{\gamma}_3\mathbf{H}_{qq}^H+\boldsymbol{\gamma}_2\mathbf{H}_{pq}\boldsymbol{\gamma}_1+\boldsymbol{\gamma}_1\mathbf{H}_{pq}\boldsymbol{\gamma}_2)/4$$

$$\boldsymbol{\varphi}_4=(\mathbf{H}_{qq}\boldsymbol{\varphi}_3+\boldsymbol{\gamma}_3\mathbf{H}_{pq}+\boldsymbol{\gamma}_2\mathbf{H}_{pq}\boldsymbol{\varphi}_1+\boldsymbol{\gamma}_1\mathbf{H}_{pq}\boldsymbol{\varphi}_2)/4$$

The eigenvalue count and matrixes of $\mathbf{F}_{0,h}^l$, $\mathbf{G}_{0,h}^l$ and $\boldsymbol{Q}_{0,h}^l$ in sublayer l can be recursively calculated as follows

$$\mathbf{F}_{0,h}^l=\mathbf{F}_{0,h}^{l+1}(\mathbf{I}+\mathbf{G}_{0,h}^{l+1}\boldsymbol{Q}_{0,h}^{l+1})^{-1}\mathbf{F}_{0,h}^{l+1} \tag{C5}$$

$$\mathbf{G}_{0,h}^l=\mathbf{G}_{0,h}^{l+1}+\mathbf{F}_{0,h}^{l+1}((\mathbf{G}_{0,h}^{l+1})^{-1}+\boldsymbol{Q}_{0,h}^{l+1})^{-1}(\mathbf{F}_{0,h}^{l+1})^H \tag{C6}$$

$$\boldsymbol{Q}_{0,h}^l=\boldsymbol{Q}_{0,h}^{l+1}+(\mathbf{F}_{0,h}^{l+1})^H(\mathbf{G}_{0,h}^{l+1}+(\boldsymbol{Q}_{0,h}^{l+1})^{-1})^{-1}\mathbf{F}_{0,h}^{l+1} \tag{C7}$$

and

$$J_{0,h}^l(D_2^0;k)=2J_{0,h}^{l+1}(D_2^0;k)+s[((\mathbf{G}_{0,h}^{l+1})^{-1}+\boldsymbol{Q}_{0,h}^{l+1}+(\mathbf{F}_{0,h}^{l+1})^H(\mathbf{G}_{0,h}^{l+1})^{-1}\mathbf{F}_{0,h}^{l+1})] \tag{C8}$$

where $l=\mathrm{N}-1,\cdots,1,0$.

References:

[1] Zhong W X, Zhong X X. Method of separation of variables and Hamiltonian system [J]. *Numerical Methods for Partial Differential Equations*, 1993, **9**(1):63-75.

[2] Zhong W X. Plane elasticity in sectorial domain and the Hamiltonian system [J]. *Applied Mathematics and Mechanics*, 1994, **15**(12):1113-1123.

[3] Zhong W X. *A New Systematic Methodology for Theory of Elasticity* [M]. Dalian: Dalian University of Technology Press, 1995.

[4] Yao W A, Zhong W X, Lim C W. *Symplectic Elasticity* [M]. New Jersey: World Scientific, 2009.

[5] Yao W A, Yang H T. Hamiltonian system based Saint Venant solutions for multi-layered composite plane anisotropic plates [J]. *International Journal of Solids and Structures*, 2001, **38**(32-33):5807-5817.

[6] Wu Q, Gao Q. The symplectic approach for analytical solution of micropolar plane stress problem [J]. *International Journal of Solids and Structures*, 2023, **264**:112095.

[7] Zhong W X, Yao W A. The Saint Venant solutions of multi-layered composite plates [J]. *Advances in Structural Engineering*, 1997, **1**(2):127-133.

[8] Li R, Tian Y, Wang P C, et al. New analytic free vibration solutions of rectangular thin plates resting on multiple point supports [J]. *International Journal of Mechanical Sciences*, 2016, **110**:53-61.

[9] Li R, Wang B, Li G, et al. Hamiltonian system-based analytic modeling of the free rectangular thin plates' free vibration [J]. *Applied Mathematical Modelling*, 2016, **40**(2):984-992.

[10] Xiong S, Zheng X R, Zhou C, et al. Buckling of non-Lévy-type rectangular thick plates: New benchmark solutions in the symplectic framework [J]. *Applied Mathematical Modelling*, 2024, **125**:668-686.

[11] Lim C W, Lü C F, Xiang Y, et al. On new symplectic elasticity approach for exact free vibration solutions of rectangular Kirchhoff plates [J]. *International Journal of Engineering Science*, 2009, **47**(1):131-140.

[12] Gao Q, Lin J H, Zhong W X, et al. A precise numerical method for Rayleigh waves in a stratified half space [J]. *International Journal for Numerical Methods in Engineering*, 2006, **67**(6):771-786.

[13] Gao Q, Zhong W X, Howson W. A precise method for solving wave propagation problems in layered anisotropic media [J]. *Wave Motion*, 2004, **40**(3):191-207.

[14] Gao Q, Yan B, Zhang Y. An accurate method for dispersion characteristics of surface waves in layered anisotropic semi-infinite spaces [J]. *Computers & Structures*, 2023, **276**:106956.

[15] Gao Q, Zhang Y H. Stable and accurate computation of dispersion relations for layered waveguides, semi-infinite spaces and infinite spaces [J]. *Journal of Vibration and Acoustics*, 2019, **141**(3):031012.

[16] Zhang T. Symplectic analysis for wrinkles: A case study of layered neo-hookean structures [J]. *Journal of Applied Mechanics*, 2017, **84**(7):071002.

[17] Sui J J, Chen J B, Zhang X X, et al. Symplectic analysis of wrinkles in elastic layers with graded stiffnesses [J]. *Journal of Applied Mechanics*, 2019, **86**(1):011008.

[18] Zhang Y H, Gao Q. A generalized method for dispersion analysis of guided waves in multilayered anisotropic magneto-electro-elastic structures [J]. *Shock and Vibration*, 2022, **2022**:1-16.

[19] Wang Q M, Tahir M, Zhang L, et al. Electro-creasing instability in deformed polymers: Experiment and theory [J]. *Soft Matter*, 2011, **7**(14):6583-6589.

[20] Wang Q M, Zhang L, Zhao X H. Creasing to cratering instability in polymers under ultrahigh electric fields [J]. *Physical Review Letters*, 2011, **106**(1):118301.

[21] Charoen-Rajapark P, Clarke D R. Confocal microscopy observations of electrical pre-breakdown of bi-layer elastomer dielectrics [J]. *Extreme Mechanics Letters*, 2021, **49**:101473.

[22] Yang S Y, Sharma P. A tutorial on the stability and bifurcation analysis of the electromechanical behaviour of soft materials [J]. *Applied Mechanics Reviews*, 2023, 75(4):044801.

[23] Wang Q M, Zhao X H. Creasing-wrinkling transition in elastomer films under electric fields [J]. *Physical Review E*, 2013, **88**(4):042403.

[24] Wang Q M, Gossweiler G R, Craig S L, et al. Cephalopod-inspired design of electro-mechano-chemically responsive elastomers for on-demand fluorescent patterning [J]. *Nature Communications*, 2014, **5**:4899.

[25] Hutchinson J W. Surface instabilities of constrained elastomeric layers subject to electro-static stressing [J]. *Journal of the Mechanics and Physics of Solids*, 2021, **153**:104462.

[26] Hutchinson D J W, Huang R, Landis C M. Errata: Surface instabilities of constrained elastomeric layers subject to electro-static stressing by J.W. Hutchinson, J. Mech. Phys. Solids 153 (2021) 104462 [J]. *Journal of the Mechanics and Physics of Solids*, 2022, **160**:104809.

[27] Huang R. Electrically induced surface instability of a conductive thin film on a dielectric substrate [J]. *Applied Physics Letters*, 2005, **87**(15):151911.

[28] Park H S, Wang Q M, Zhao X H, et al. Electromechanical instability on dielectric polymer surface:

Modeling and experiment [J]. *Computer Methods in Applied Mechanics and Engineering*, 2013, **260**: 40-49.
[29] Landis C M, Huang R, Hutchinson J W. Formation of surface wrinkles and creases in constrained dielectric elastomers subject to electromechanical loading [J]. *Journal of the Mechanics and Physics of Solids*, 2022, **167**: 105023.
[30] Suo D Z. Theory of dielectric elastomers [J]. *Acta Mechanica Solida Sinica*, 2010, **23**(6): 549-578.
[31] Dorfmann A, Ogden R W. Nonlinear electroelasticity [J]. *Acta Mechanica*, 2005, **174**(3): 167-183.
[32] Dorfmann A, Ogden R W. Nonlinear electroelastostatics: Incremental equations and stability [J]. *International Journal of Engineering Science*, 2010, **48**(1): 1-14.
[33] Dorfmann L, Ogden R W. Instabilities of an electroelastic plate[J]. *International Journal of Engineering Science*, 2014, **77**: 79-101.
[34] Zhong W X, Williams F W, Bennett P N. Extension of the Wittrick-Williams algorithm to mixed variable systems [J]. *Journal of Vibration and Acoustics*, 1997, **119**(3): 334-340.
[35] Rudykh S, DeBotton G. Stability of anisotropic electroactive polymers with application to layered media [J]. *Zeitschrift Für Angewandte Mathematik Und Physik*, 2011, **62**(6): 1131-1142.
[36] Bahreman M, Arora N, Darihani H, et al. Structural and material electro-mechanical instabilities in microstructured dielectric elastomer plates [J]. *European Journal of Mechanics-A/Solids*, 2022, **94**: 104534.
[37] Bertoldi K, Gei M. Instabilities in multilayered soft dielectrics [J]. *Journal of the Mechanics and Physics of Solids*, 2011, **59**(1): 18-42.
[38] Furer J, Castañeda P P. Macroscopic instabilities and domain formation in neo-Hookean laminates [J]. *Journal of the Mechanics and Physics of Solids*, 2018, **118**: 98-114.
[39] Lopez-Pamies O, Castañeda P P. Microstructure evolution in hyperelastic laminates and implications for overall behavior and macroscopic stability [J]. *Mechanics of Materials*, 2009, **41**(4): 364-374.
[40] Kyriakides S, Arseculeratne R, Perry E J, et al. On the compressive failure of fiber reinforced composites [J]. *International Journal of Solids and Structures*, 1995, **32**(6-7): 689-738.
[41] Pane I, Jensen H M. Plane strain bifurcation and its relation to kinkband formation in layered materials [J]. *European Journal of Mechanics-A/Solids*, 2004, **23**(3): 359-371.
[42] Castañeda P P. Soft elastic composites: Microstructure evolution, instabilities and relaxed response by domain formation [J]. *European Journal of Mechanics-A/Solids*, 2023, **100**: 105033.
[43] Triantafyllidis N, Maker B N. On the comparison between microscopic and macroscopic instability mechanisms in a class of fiber-reinforced composites [J]. *Journal of Applied Mechanics*, 1985, **52**(4): 794-800.
[44] Pathak P, Arora N, Rudykh S. Magnetoelastic instabilities in soft laminates with ferromagnetic hyperelastic phases [J]. *International Journal of Mechanical Sciences*, 2022, **213**: 106862.
[45] Chen V W, Arora N, Goshkoderia A, et al. Mechanical instability tuning of a magnetorheological elastomer composite laminate [J]. *Composites Part B: Engineering*, 2023, **251**: 110472.
[46] Rudykh S, Bertoldi K. Stability of anisotropic magnetorheological elastomers in finite deformations: A micromechanical approach [J]. *Journal of the Mechanics and Physics of Solids*, 2013, **61**(4): 949-967.

基于辛本征值方法的受约束介电弹性体中褶皱不稳定性的分析

张 腾*

(雪城大学 机械与航空系, 美国纽约, NY 13244)

摘 要: 辛弹性力学已广泛应用于弹性学中各种边值问题的精确解、计算表面波模式以及预测多层超弹性薄膜中的表面褶皱。本文展示了辛分析框架还可应用于受约束介电弹性体中的表面褶皱。机械和电位移向量是两个基本变量来描述介电弹性体中机械变形与电场紧密耦合。褶皱的临界电压可以通过引入基本变量的对偶变量来从辛本征值问题中解决。本文采用扩展的 W-W(Wittrick-Williams)算法和精确的积分方法,准确而高效地解决制定的辛本征值问题的本征值。通过将褶皱电压和波数与有无表面能的褶皱基准结果进行比较,验证了辛分析的有效性。辛分析框架简洁且适用于其他不稳定问题,如分层电介质弹性体、磁弹性不稳定性以及层压复合结构的微观和宏观不稳定性。

关键词: 辛; 介电弹性体; 褶皱; 本征值分析

中图分类号: O343.9 **文献标志码**: A **文章编号**: 1007-4708(2024)01-0209-08

收稿日期: 2023-11-08; **修改稿收到日期**: 2023-11-24.

作者简介: 张 腾* (1985-), 男, 博士, 副教授(E-mail: tzhang48@syr.edu).

引用本文/Cite this paper:

张 腾. 基于辛本征值方法的受约束介电弹性体中褶皱不稳定性的分析[J]. 计算力学学报, 2024, **41**(1): 209-216.

ZHANG Teng. Analyzing wrinkling instabilities in constrained dielectric elastomers: A symplectic eigenvalue approach [J]. *Chinese Journal of Computational Mechanics*, 2024, **41**(1): 209-216.